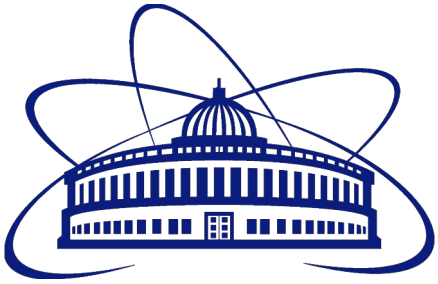

JOINT INSTITUTE FOR NUCLEAR RESEARCH
Dzhelepov Laboratory of Nuclear Problems

Radiation Protection And The Safety Of The Radiation Sources

Supervisor:
Dr. Said Abou El-Azm
Dzhelepov Laboratory of Nuclear Problems, JINR

Student:
Zeyad Mansour B. Radwan
Cairo University

Participation date: October 30 – November 30, Wave 13

Dubna, 2025

Table of Contents

Table of Figures

Index of Tables

1. Abstract

Ionizing radiation is used in a plethora of fields such as medical and environmental applications, and in a lot of those fields, simple detection of presence of radiation is not enough. Calibration and identification of radioactive sources are crucial, and for medical applications, knowing how a material block radiation is also very important for the safety of the staff. In our course, we will use softwares such as ROOT, SRIM, and others to identify unknown sources, calibrating/ optimizing detectors, and compare detectors based on their resolution. The report will include scintillating detectors such as BGO and Nai(Tl), and solid state detector such as CdTe. Finally, we will determine the attenuation coefficient for Al and Cu, and perform monte carlo simulation to correlate with experimental data on alpha particle trajectories through air.

2. Introduction

Radiation is the propagation of energy through space in the form of electromagnetic waves or fast moving particles. Electromagnetic radiation (photons) energy is determined by the electric and magnetic field oscillation frequency through space —calculated with E=hv, while a fast moving particle radiation energy is estimated by its kinetic energy (K.E.). Radiation is broadly classified by its ability to ionize atoms into **ionizing** and **non-ionizing** radiation.

Ionizing Radiation consists of high energy photons of high frequencies or fast-moving particles of high K.E. that are very detrimental to biological systems due to their ability to form free-radicals insides the cells that greatly inhibit normal cellular functions and induce cross-linking between important cellular macromolecules. An example of ionizing radiation are X-Rays, Gamma-Rays, and fast-moving particles such as alpha radiation in the form of helium nuclei, beta radiation in the form of high K.E. electrons, Proton radiation, Neutron radiation, and Positrons radiation. Ionizing radiation is absorbed by the material being bombarded through different mechanisms based on their energy and type. They can be absorbed through the electron cloud in different molecular orbitals in the form of ionization (The atom loses or gains an electron) or excitation (The electron transition from one molecular orbital to another); or through the atom's nucleus, which can make it unstable and become radioactive in some cases in what is known as **induced radioactivity.**

Non-ionizing Radiation, however, is not as harmful as its ionizing counterpart due its lack of significant energy needed to knock electrons off from their atoms and thereby doesn't form free radicals inside living tissue. Materials do absorb the non-ionizing radiation energy through their electron cloud and release this excess energy in the form of emitted light (fluorescence and phosphorescence), heat, or change in their vibration/rotational mode of their atoms or bonds. Concentrating non-ionizing radiation in a living tissue is very detrimental to said tissue because of the excess heat generated inside cells. Examples of non-ionizing radiation include low frequency ultraviolet light (UV-A), visible light, infrared, microwaves, and radio-waves. It's worth noting that although UV is considered non-ionizing in many textbooks, they can however form free-radicals if their energy is high enough (UV-B and UV-C), and UV in general is considered carcinogenic.

Different types of radiation have varying levels of penetration through mediums based on how they interact with matter. For example, radio-waves have very long wavelength that they hardly interact with atoms in material with moderate thickness, and they are not energeticenough to excite atoms in it, so they mostly pass through; while radiation of small

wavelength (high frequency) can interact with the atom's electrons cloud and thus have variation in their penetration power based on how well they interact with the electron cloud. High speed particles on the other hand are generally the least capable in penetrating mediums because they rapidly dissipate their energy to the medium's atoms/molecules through physical collisions. The notion of 'penetration power' is better known as **attenuation.**

The amount of energy absorbed by a material (i.e. dosage) was estimated in many different ways in the past before the SI units were fully implemented around the world. There were the röntgen, rads, rems, and as funny as it may sound, the banana equivalent dose. Currently, however, the dose of absorbed energy is calculated using the **gray (Gy)**, which measures the amount of energy in terms of Joules/Kg of material.

For biological research, the usage of the gray for all radiation types was unreliable, as different radiation types transfer energy in different manners to one another, which introduces us to the **equivalent dose** or **sieverts (Sv)**. sieverts puts weight to the type of radiation to better reflect how damaging (in a sense) the absorbed energy was on the tissue. For example, 1 Gray of X-ray is 1 sieverts, while 1 Gray of Alpha radiation is 20 sieverts. It was later noted that different parts of the body absorb ionizing radiation differently from one another because of their water, fat, or protein content; and therefore, an additional weighing factor was added when measuring the 'impact' of the absorbed radiation on the specific tissue, in what is known as the **effective dose,** which is also measured in sieverts but with the added nuance of the additional tissue-specific weight.

Accurate detection and differentiation of ionizing radiation is essential in different fields, especially in environmental monitoring and biological research. There are many type of detectors that are able to detect ionizing radiation and measure their energy with varying accuracy and precision, and they are broadly categorized into gas-based, scintillating crystal-based, semi-conductor-based (solid state detector), or other less conventional methods such as thermoluminescent and gel/film-dosimeters. Each method of detection gives a different picture on the type and/or energy of the ionization radiation, and thus are used in specific setups based on what the researchers are trying to study. For our purposes of identifying an unknown radioactive source, measure the energy of the ionizing radiation in an energy-dispersive manner, and estimating the attenuation of a material; we will focus on scintillator-types and solid-state detectors.

Scintillator detectors are crystals that emit light when under irradiation, where the amount of light they produce is proportional to the energy/amount of the radiation. Scintillators are easy to make and are of good sensitivity and accuracy for most applications, but they might be challenging to properly setup because of the needed photomultiplier and electronics that are needed to accurately produce and interpret data. Examples of scintillator detectors are **Bismuth Germanate (BGO),** and **thallium-activated sodium iodide (NaI[Tl])**.

Gas-based detectors use vapors that ionizes when radiation passes through, and that small trail of ions can pass electrical current for a moment. With calibration, this can be used to accurately measure radiation energy and in some cases, types of radiation.

Solid-state detectors are currently the frontier of ionizing radiation detection, and it focuses on the fact that ionizing radiation produces electron-holes in semi-conductor that can be measured accurately. Solid-state detectors can be made of a large array of semi-conductor (known as Pixel detectors) such as doped **silicon** (Si) or c**admium telluride** (CdTe) with all the necessary electronics integrated with it. The biggest challenge with such solid-state detectors is calibrating the huge number of the 'pixels' inside the array of semi-

conductors to give proper readings on energy of the radiation. It's important to note that not all solid-state detectors are Pixel detectors.

In this report, we will focus on data that were brought from **BGO and NaI(Tl) scintillating detectors,** as well as the solid-state **CdTe** detector.

3. Tasks

Our aim is to familarise ourselves with the idea of identifying unknown sources, calibrating our detectors, estimating resolution, studying the effect of voltage of the photomultiplier in scintillating-type detection, and measuring attenuation coefficient for different sheilding matercopper and aluminum. We will also aim to showcase how fast-moving particles like alpha radiation dissipate their energy quickly in mediums like air using monte-carlo simulations.

3.1. Task 1.: Effect on Resolution of BGO Detectors due to Voltage change

BGO detector resolution (as well as other scintillating detectors) depend heavily on the photomultiplier applied voltage, where a higher voltage works best to resolve overlapping peaks. For our task, different voltages were applied to the photomultiplier coupled to the BGO crystal and Co^{60} source was placed against it. The resulting data brought from the DRS4 circuit (which is responsible for the energy dispersive data collection method from the photomultiplier) was evaluated using ROOT program and gaussian fitting was done on the significant Co^{60} peak (figure 1). This was done multiple times at different voltages, and the mean and spread of the peak was calculated on the same program (table 1).

Resolution % was calculated following the equation:

$$R\% = \frac{\sigma}{\mu} 2.23 \times 100$$

Where the number 2.23 is the product of calculating full width at half maximum FWHM for a Gaussian peak using the following equation:

$$FWHM = 2\sqrt{2\ln 2}\,\sigma \approx 2.355\,\sigma$$

Where σ: Standard deviation

μ: Centroid Mean Channel Number

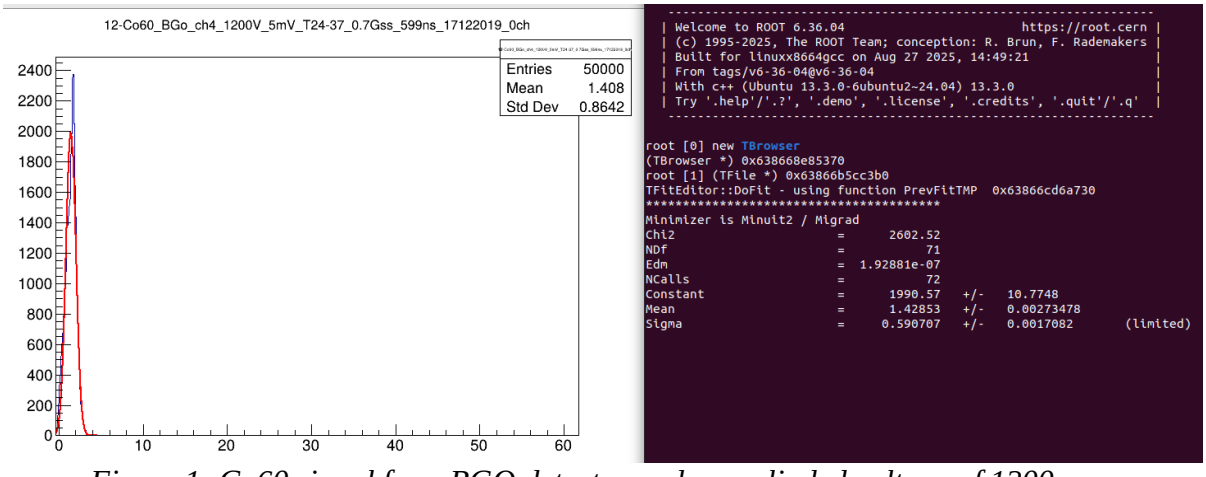

Figure 1: Co60 signal from BGO detector under appliaded voltage of 1200 Volts

Table 1: Effect of photomultiplier applied voltage on resolution of the BGO detector

n	Voltage (V)	Centroid Mean (μ)	Sigma (∑)	Constant	Resolution (%)
1	1200	1.42841	0.590511	2411.73	97.36
2	1300	1.82	0.489616	3822.94	63.35
3	1400	1.924	0.39	3330	47.74
4	1500	3.015	0.39776	5973	31.07
5	1600	4.39	0.6	5495	32.19
6	1700	6.1	0.707	4898.15	27.29
7	1900	10.42	1.03519	1672	23.4
8	2000	13.57	1.32041	1680	22.92

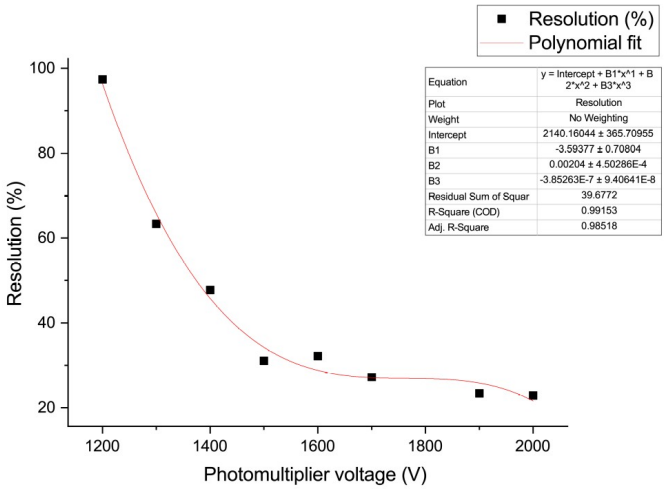

Figure 2: Photomultiplier applied voltage effects on resolution

It's revealed from the previous test that higher applied voltage across the photomultiplier will increase the resolution by decreasing the the full width at half maximum significantly, which will help in resolving overlapping peaks in the next test.

3.2. Task 2: Energy Calibration of BGo detectors & Determine Unknown sources

Calibration of BGO detectors was completed using a Co^{60} and a Cs^{137} source, which give intense peaks at certain (known) energies that are specific for the Co^{60} and Cs^{137} atom' emission energies of gamma ray.

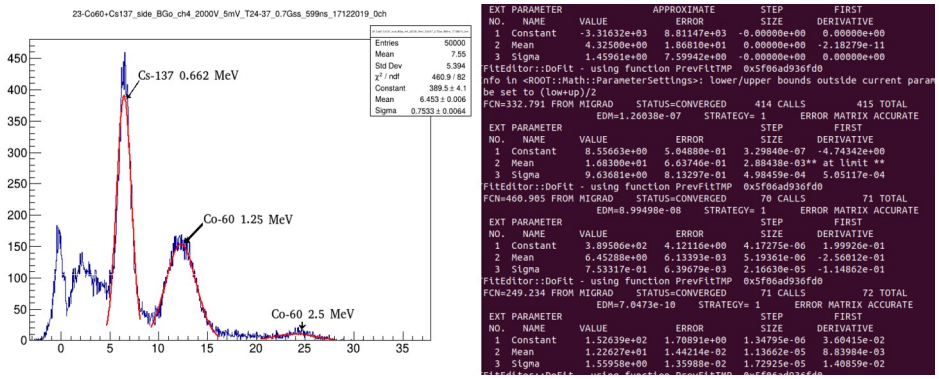

Figure 3: Calibration of BGO detector usign Cs137 and Co60 soruces.

The channel numbers that received the signal peak were averaged and were assigned as a way to approximate energy with the new calibration curve made from the previous graph.

Table 2: Channel number mean correlate to energy

n	energy	mean (channel)	sigma
1	0.662	6.4528	0.753317
2	1.25	12.2627	1.55958
3	2.5	24.39667	2.02318

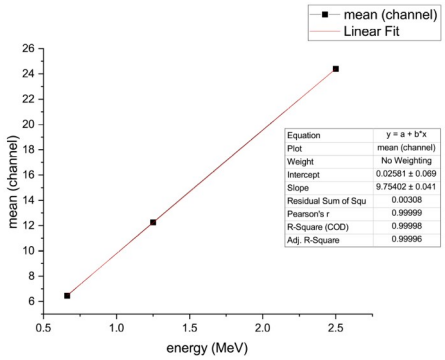

Figure 4: BGO detector calibration curve

Using this curve, we will be able to relate peaks at any given channel to energy in MeV, as the energy from the linear equation curve is:

$$Energy = \left(\frac{Channel\ No\ Mean}{9.75404}\right) - 0.02581$$

A mix unknown radiation sources were then placed on the same detector, and using the previous calibration curve, will try to best estimate which radioactive isotope is present in our sample:

Figure 5: Unknown source energy dispersive spectra from BGO detector

Using the previous equation, we will estimate mean channel number where the highest peak was taken and relate it to the energy of incident particle, and we used the energy to assume possible isotope based on half-life (in routine environmental analysis, we rarely focus on isotopes that have half life of few days or hours, as those are most likely man-made) and used the data from the **NuDat database**: https://www.nndc.bnl.gov/nudat3/indx_dec.jsp. This will give us the following table:

Table 3: Possible radioactive isotopes

Peak No.	Energy (MeV)	Possible Source
1	0.1032	Au-95, Eu-152, Thr-230, or Thr-232
2	0.0569	Am-241
3	0.0464	Pb-214
4	0.0365	I-125
5	0.0270	Sm-151
6	0.1901	Ra-226 or U-235
7	0.2834	Ba-133
8	0.1300	Eu-152 or Co-57
9	0.2300	U-238 decay products

Note that these energies could come from gamma rays, x-rays, alpha, or beta radiation. Thus, for robust investigations depending on the needed application, higher caliber equipment will be used, but of casual environmental screening, this will work fine.

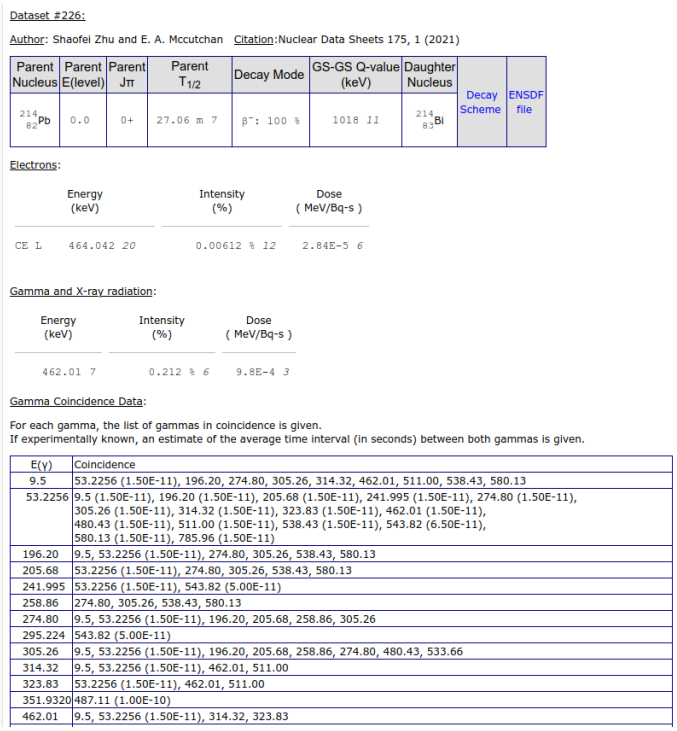

Dataset #226:

Author: Shaofei Zhu and E. A. Mccutchan Citation:Nuclear Data Sheets 175, 1 (2021)

Parent Nucleus	Parent E(level)	Parent Jπ	Parent $T_{1/2}$	Decay Mode	GS-GS Q-value (keV)	Daughter Nucleus	Decay Scheme	ENSDF file
$^{214}_{82}$Pb	0.0	0+	27.06 m 7	β⁻: 100 %	1018 11	$^{214}_{83}$Bi		

Electrons:

Energy (keV)	Intensity (%)	Dose (MeV/Bq-s)
CE L 464.042 20	0.00612 % 12	2.84E-5 6

Gamma and X-ray radiation:

Energy (keV)	Intensity (%)	Dose (MeV/Bq-s)
462.01 7	0.212 % 6	9.8E-4 3

Gamma Coincidence Data:

For each gamma, the list of gammas in coincidence is given.
If experimentally known, an estimate of the average time interval (in seconds) between both gammas is given.

E(γ)	Coincidence
9.5	53.2256 (1.50E-11), 196.20, 274.80, 305.26, 314.32, 462.01, 511.00, 538.43, 580.13
53.2256	9.5 (1.50E-11), 196.20 (1.50E-11), 205.68 (1.50E-11), 241.995 (1.50E-11), 274.80 (1.50E-11), 305.26 (1.50E-11), 314.32 (1.50E-11), 323.83 (1.50E-11), 462.01 (1.50E-11), 480.43 (1.50E-11), 511.00 (1.50E-11), 538.43 (1.50E-11), 543.82 (6.50E-11), 580.13 (1.50E-11), 785.96 (1.50E-11)
196.20	9.5, 53.2256 (1.50E-11), 274.80, 305.26, 538.43, 580.13
205.68	53.2256 (1.50E-11), 274.80, 305.26, 538.43, 580.13
241.995	53.2256 (1.50E-11), 543.82 (5.00E-11)
258.86	274.80, 305.26, 538.43, 580.13
274.80	9.5, 53.2256 (1.50E-11), 196.20, 205.68, 258.86, 305.26
295.224	543.82 (5.00E-11)
305.26	9.5, 53.2256 (1.50E-11), 196.20, 205.68, 258.86, 274.80, 480.43, 533.66
314.32	9.5, 53.2256 (1.50E-11), 462.01, 511.00
323.83	53.2256 (1.50E-11), 462.01, 511.00
351.9320	487.11 (1.00E-10)
462.01	9.5, 53.2256 (1.50E-11), 314.32, 323.83

Figure 6: Screening for possible elements that correspond to the energy we detecting from our detector. Data fetched from NuDat database.

3.3. Task 3: Calibration, Resolution and Find Unknown Sources for NaI Detector

Activated sodium iodide with thallium (NaI[Tl]) is perhaps the most popularly used scintillating detector. It’s relatively simple to manufacture, cheap, and reliable for many applications.

The working principle of **NaI(Tl)** is basically the same as **BGO** detectors; the crystal emits light of specific wavelengths upon irradiation with ionizing radiation (which can be x-rays, gamma rays, alpha radiation, beta radiation, etc..), and a photomultiplier collects the

resulting photons, amplifies it and directs it to **DRS4** circuit, which contains thousands of small amplifiers that are gated with a switch that open/close to collect the amplified signal from the photomultiplier at specific time intervals. The switches then open and release the charge stored within the capacitors, which are interpreted by other components and software (like multichannel analyzer -MCA) to give the histograms we saw earlier.

For this test, we will basically do the same thing we did before with the BGO detector, forming a calibration curve, and identifying unknown sources using NuDat database or others.

To measure voltage effects on resolution of the detector, different voltages were applied to the photomultiplier and a peak was tracked in each different voltage. Channel mean, standard deviation, and peak height were record using ROOT program as follows

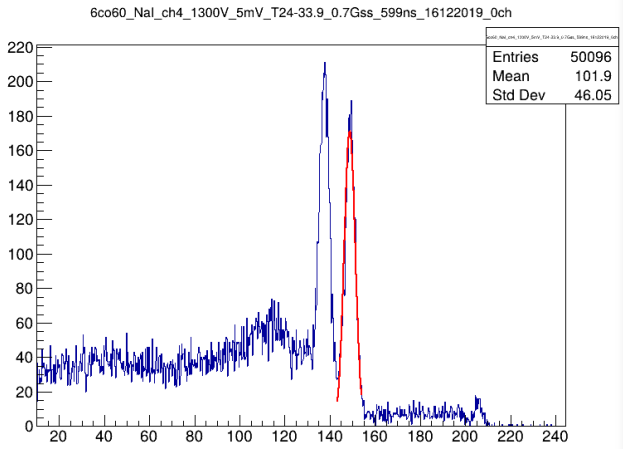

Figure 7: NaI detector spectra for Co60 source under applied voltage of 1300 V.

This was done multiple times for each voltage on the same peak we choose, which will give us these results:

Table 4: NaI detector voltage effect on resolution.

n	Voltage (V)	Centroid Mean (μ)	Sigma (∑)	Constant	Resolution%
1	900.00	26.65	0.50	1,161.00	4.18
2	1,000.00	45.37	0.82	472.00	4.03
3	1,100.00	73.27	1.56	137.64	4.76
4	1,200.00	108.54	1.74	153.00	3.57
5	1,300.00	148.80	2.28	182.00	3.41

Note that a higher voltage doesn't necessary make a linear relation with resolution for every peak, as for our example in our selected peak, the point 1100 V has a higher resolution % compared to other point, which means we will not use this voltage for our analysis (or at least for detecting this peak in specific). It's also worth to note that at relatively low voltage from that used in the BGO detector, NaI detector was able to have far better resolving power; which showcases the difference between the two detectors.

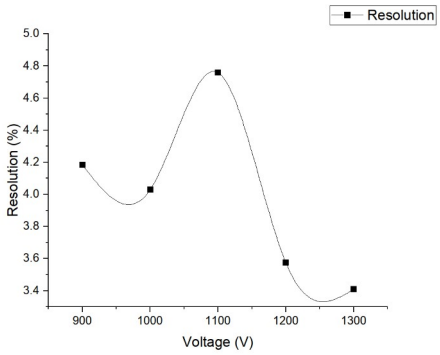

Figure 8: Resolution% against applied voltage for NaI detector.

For calibrating a sodium iodide detector, we will follow the same tactic as before with BGO detector using a Co^{60} and Cs^{137} source with known relative peak positions and assign each peak to its corresponding energy fetched from NuDat database or other.

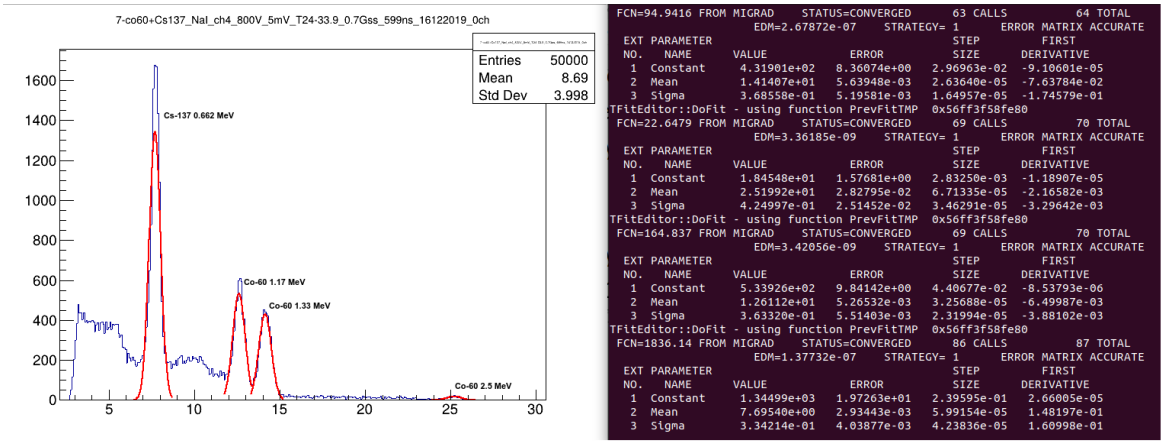

Figure 9: Calibration of NaI detector using Co60 and Cs137 radioactive soruces.

This will give us the following data:

Table 5: Calibration table for NaI detector

n	Mean (μ)	Sigma (∑)	Constant	Energy (MeV)
1	7.6954	0.334214	1344.99	0.662
2	12.6112	0.36332	533.926	1.17
3	14.1407	0.368558	431.901	1.33
4	25.1992	0.424997	18.4548	2.5

Note the splitting in the previously defined 1.25 MeV peak in the BGO detector to a more resolved 1.17 & 1.33 MeV.

And plotting that, we get:

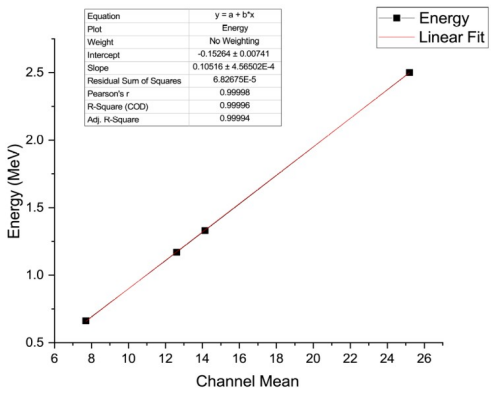

Figure 10: Calibration curve for NaI detector.

Now that the calibration curve is made, the linear equation for it will be used to correlate mean channel number to energy in MeV; which will be:

$$Energy = -0.15264 + 0.10516\, Ch_{mean}$$

We can now begin identifying unknown sources using this calibration curve as follows:

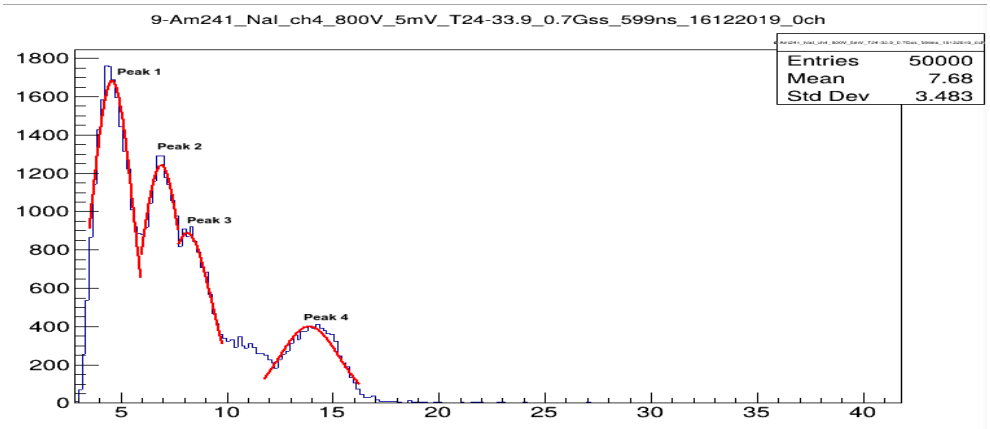

Figure 11: Identification of unknown radio-source using NaI Detector.

Table 6: Energy spectra of Am241

n	Mean (μ)	Energy (MeV)
1	4.60	0.33
2	6.91	0.57
3	8.14	0.70
4	13.88	1.31

The spectrum is that of the gamma spectrum of Am241 & Am243.

It should be noted that complete identification using this method for a sample that has mixed source may not be easily identifiable without additional information from heavier equipment like XRF or such.

3.4. Task 4: Calibration, Resolution for CdTe Detector

CdTe detector is a solid state, semi-conductor type detector that does not rely on a photomultiplier to generate the needed peaks, instead works by measuring the amount of electron-hole pairs that are generated when the semi-conducting material is bombarded with ionizing radiation. The CdTe detector is more suitable to detect X-rays, as X-rays form more electron-hole pairs than gamma radiation, but it can still be used to detect a wide range of ionizing radiation. CdTe, since its a semi-conducting, is able to work at room temperature without liquid nitrogen cooling

CdTe was calibrated using known peaks from Co57 and Am241, and a calibration curve was done as follows:

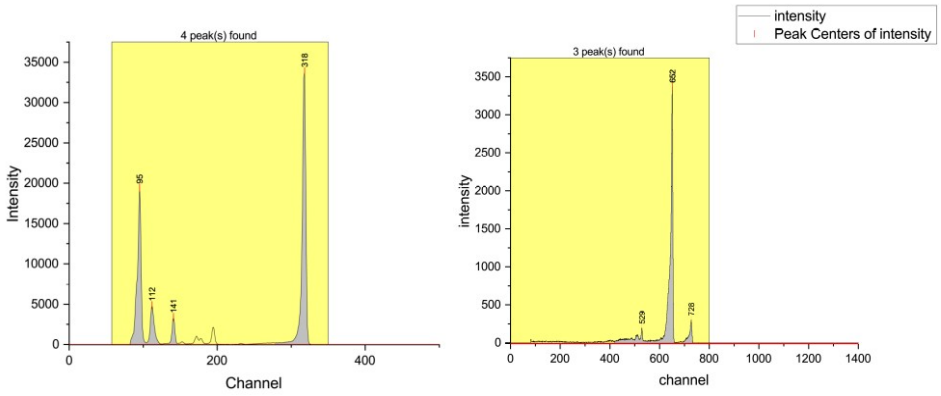

Figure 12: CdTe detector showcasing Co57 (Right) and Am241 (Left) energy spectra.

Table 7: CdTe detector data for calibration.

n	Channel mean	FWHM	Constant	Area	Energy (KeV)	R%	Element
1	95	4.7307	19461	118087.5	13.9	4.98	Am-241
2	112	5.48194	4882	30667.5	17.7	4.89	Am-241
3	141	3.96589	3419	15045	20.8	2.81	Am-241
4	318	4.81819	33894	200551	59.54	1.52	Am-241
5	529	26.0156	194	6749.5	-	-	KX escape peak
6	652	7.41122	3371	410944	122	1.14	Co-57
7	728	7.77028	303	3662.5	136.5	1.07	Co-57

Note that peak number 5 on the Co57 graph is merely an escape peak signal, that is, an artifact X ray signal that was generated on the detector itself, and thus will be omitted from the calibration curve. Also note that CdTe has the lowest resolution when compared to the scintillating detectors.

This will give us the following:

From there, we can derive the linear equation that correlates the average channel number to energy:

$$Energy = -4.5589 + 0.1944 \times Channel_{avg}$$

Now that the CdTe detector is calibrated, we can now use it to identify unknown radioactive sources as before.

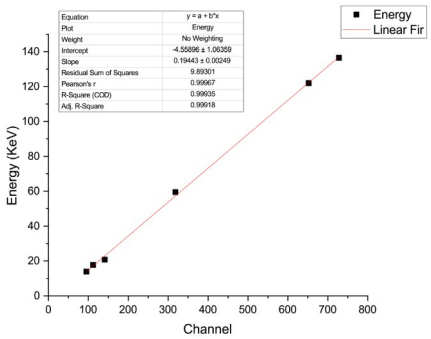

Figure 13: Calibration curve for CdTe.

3.5. Task 5: Attenuation Coefficients Using Am-241 source and Registration efficiency

The attenuation coefficient is a **constant** that is used to describe how well a material will block an energetic incident particle/photon from passing through it, and it's a very important concept when dealing with radiation shielding. The attenuation coefficient is a calculated by placing a material of varying length against a detector (NaI for our case) and measure a peak intensity for each material thickness, then following the equation,

$$I = I_0 e^{-x\mu}$$

Where;

I: Is the beam intensity that passed through the material

I_0: Is the incident beam intensity (without anything in its path)

x: Linear attenuation coefficient

μ: Material thickness

which can be further refined into:

$$\frac{I}{I_0} = e^{-x\mu}$$

$$\ln\frac{I}{I_0} = \ln e^{-x\mu}$$

$$\ln\frac{I}{I_0} = -x\mu$$

$$-\left(\ln\frac{I}{I_0}\right) = x\mu$$

we can determine the constant x for this specific material. The shielding material in our case will be either aluminum or copper, and will be set-up with the following configuration (with attention to safety and proper operation of electronics using lead housing) using Am241 source and CdTe or NaI(Tl) detector:

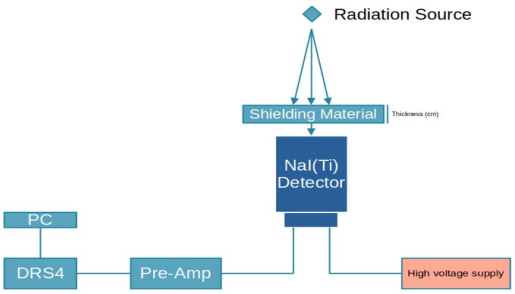

Figure 14: Example of a scintillation detector setup.

For **aluminum** sheet, as the thickness is varied, the I/I_0 varies as well, giving us the following diagram representing the shielding effects of thicker aluminum sheets:

Table 8: Al thickness to detector intesity.

Thickness (cm)	I/I0
0	1
0.15	0.75573
0.3	0.72
0.45	0.70569
0.75	0.68596
0.9	0.67155
1.08	0.66103
1.26	0.64

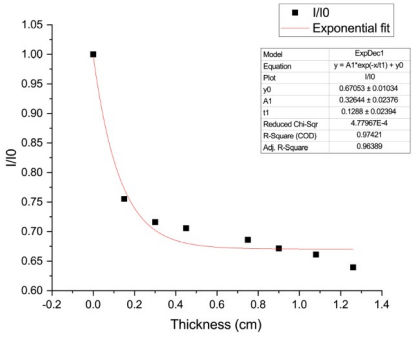

Figure 15: Al thickness to detector readings.

To get the attenuation coefficient x for aluminum in our case, we will have to follow that last equation to and form a linear function with slope equal to x by plotting $-\text{Ln}(I/I_0)$ and Thickness:

Table 9: Data transformation for Al

Thickness (cm)	-ln(I/I0)
0.00	0.00
0.15	0.28
0.30	0.33
0.45	0.35
0.75	0.38
0.90	0.40
1.08	0.41
1.26	0.45

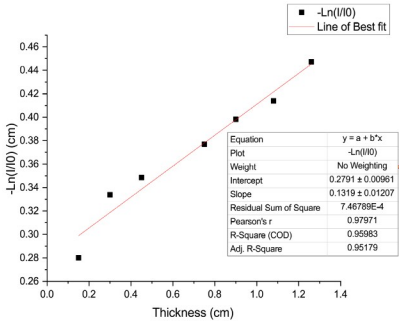

Figure 16: Transformed data for Al, slope equal to attenuation coefficient.

Note that we omitted the '0' in the plot as it heavily skews data

From the curve above, we can estimate the linear attenuation coefficient for Al as the slope, which is equal to **0.1319 ± 0.01207 cm^{-1}**

Following the same rational for **copper sheet**, we get the following:

Table 10: Copper thickness to intensity at the detector.

thickness cm	I/I0
0.00	1
0.20	0.73931
0.25	0.7357
0.40	0.68065
0.80	0.58611
1.00	0.53827
1.20	0.48

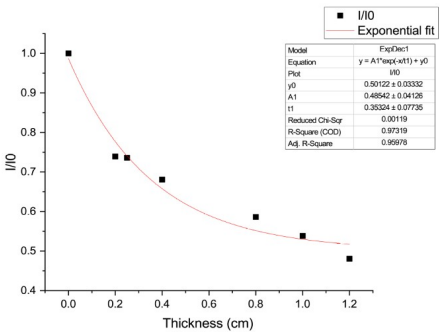

Figure 17: Copper thickness to detector reading.

We can then calculate -Ln(I/I_0) and slope as follows:

Table 11: Data transformation of Cu

thickness cm	-ln(I/I0)
0.00	0.00
0.20	0.30
0.25	0.31
0.40	0.38
0.80	0.53
1.00	0.62
1.20	0.73

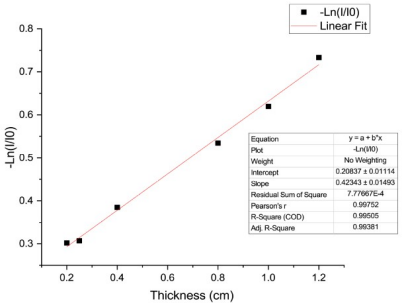

Figure 18: Transformed data against Cu thickness. Slope is the attenuation coefficient.

Note that we omitted the '0' in the plot as it heavily skews data

From the curve above, we can estimate the linear attenuation coefficient for Cu as the slope, which is equal to **0.42343 ± 0.01493 cm^{-1}**

From our results, we can conclude that copper has higher attenuation coefficient and thus better capacity to block radiation; although it should be noted that the attenuation coefficient also depends on what type of radiation is penetrating the material, for example, paper has high attenuation coefficient for alpha radiation but allows almost all gamma and x ray through (low attenuation).

3.6. Task 6: Calculating alpha radiation penetration/energy dispersion in air with SRIM program

To simulate how alpha radiation travels through mediums like air, we will use a program known as Stopping and Range of Ions in Matter (**SRIM**), which is a collection of calculations /simulations dealing with ion transport in matter. The simulation uses monte-carlo sampling to estimate the ion trajectory in the medium.

To validate the results from the simulation, we will first measure detector counts using a plastic scintillating detector at different lengths from the detector:

```
source Pu239, Energy 5.5 MeV
detector Plastic
Appiled volt 2000V
```

Table 12: Plastic detector results against Plutonium 239 isotope (alpha emitter).

Distance (cm)	Counts
0	440
0.5	390
1	320
1.5	250
2	200
2.5	150
3	100
3.5	50
3.8	25
4	0

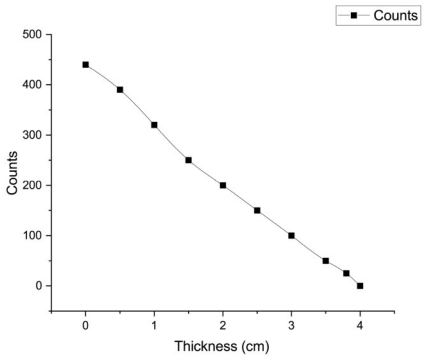

We will simulate it on SRIM using a He atom with energy of 5500 KeV, and using air from the library of mediums.
The results are as follows:

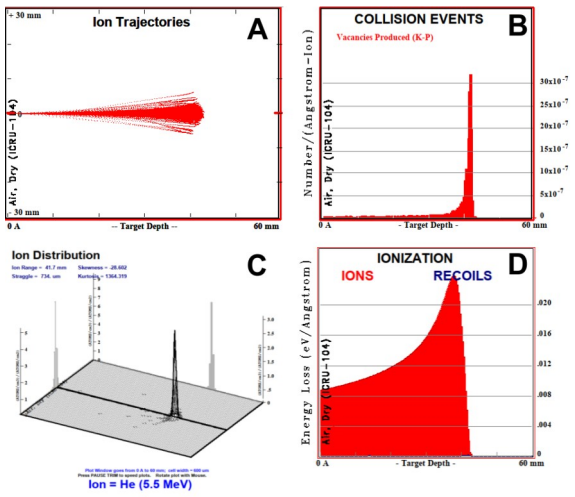

Figure 19: SRIM results. A: Ion trajectories in relation to air depth, B: Collision events, C: Ionization 3D plot in relation to depth, D: Ionization to recoil.

The figure above in section A shows the lines that represent the trajectories of alpha particles traveling through air and slowing down due to collision events, as shown in sub-figure B. The particles mostly stop at 40-50 mm, which matches our experimental results.

4. References

1. Radiation Detection and Measurement — Knoll, G. F. (2010). 4th ed. John Wiley & Sons. ISBN 978-0-470-13148-0.
2. Solid-State Radiation Detectors: Technology and Applications — Awadalla, S. (Ed.) (2015). CRC Press.
3. Tables of X-Ray Mass Attenuation Coefficients and Mass Energy-Absorption Coefficients 1 keV to 20 MeV for Elements Z = 1 to 92 and 48 Additional Substances of Dosimetric Interest — Hubbell, J. H., & Seltzer, S. M. (1995). NISTIR 5632. National Institute of Standards and Technology. https://doi.org/10.6028/NIST.IR.5632
4. SRIM — Ziegler, J. F., Ziegler, M. D., & Biersack, J. P. (2010). *SRIM – The stopping and range of ions in matter (2010)*. Nuclear Instruments and Methods in Physics Research Section B, 268(11–12), 1818–1823. https://doi.org/10.1016/j.nimb.2010.02.091
5. Growth and Evaluation of Improved CsI:Tl and NaI:Tl Scintillators — Hawrami, R., Farsoni, A., Sabet, H., & Szydel, D. (2021). arXiv preprint.